

# Tuning of a graphene-electrode work function to enhance the efficiency of organic bulk heterojunction photovoltaic cells with an inverted structure

Gunho Jo,<sup>1</sup> Seok-In Na,<sup>2</sup> Seung-Hwan Oh,<sup>3</sup> Sangchul Lee,<sup>1</sup> Tae-Soo Kim,<sup>1</sup> Gunuk Wang,<sup>1</sup> Minhyeok Choe,<sup>1</sup> Woojin Park,<sup>1</sup> Jongwon Yoon,<sup>1</sup> Dong-Yu Kim,<sup>1</sup> Yung Ho Kahng,<sup>1,3,a)</sup> and Takhee Lee<sup>1,b)</sup>

<sup>1</sup>Department of Materials Science and Engineering, Department of Nanobio Materials and Electronics, Gwangju Institute of Science and Technology, Gwangju 500-712, Republic of Korea

<sup>2</sup>Korea Institute of Science and Technology, Institute of Advanced Composite Materials, Jeollabuk-do 565-902, Republic of Korea

<sup>3</sup>Research Institute for Solar and Sustainable Energies, Gwangju Institute of Science and Technology, Gwangju 500-712, Republic of Korea

(Received 5 August 2010; accepted 17 October 2010; published online 23 November 2010)

We demonstrate the fabrication of inverted-structure organic solar cells (OSCs) with graphene cathodes. The graphene film used in this work was work-function-engineered with an interfacial dipole layer to reduce the work function of graphene, which resulted in an increase in the built-in potential and enhancement of the charge extraction, thereby enhancing the overall device performance. Our demonstration of inverted-structure OSCs with work-function-engineering of graphene electrodes will foster the fabrication of more advanced structure OSCs with higher efficiency. © 2010 American Institute of Physics. [doi:10.1063/1.3514551]

Graphene is a promising next-generation conducting material with the potential to replace traditional electrode materials such as indium tin oxide (ITO) in optoelectronic devices. It combines several advantageous characteristics including low sheet resistance, high optical transparency, and excellent mechanical properties.<sup>1,2</sup> Recent research has coincided with increased interest in the applications of graphene in displays,<sup>3</sup> light-emitting diodes,<sup>4</sup> and solar cells.<sup>5-7</sup> Until recently, only a few approaches had reported the use of graphene films as anodes in organic solar cells (OSCs) with conventional device structures.<sup>5-10</sup> However, the power conversion efficiency (PCE) of these cells was lower than the PCE of conventional ITO electrode-based OSCs. PCE improvement in graphene electrode-based OSCs can be performed through several methods; (1) improvement of graphene quality, (2) development of advanced structure OSC, and (3) interface control between the active layer and the graphene electrode.

In this letter, we demonstrate the application of graphene films as cathodes in inverted structure OSCs, which is required to increase design flexibility in building tandem or stacked OSCs that utilize solar energy more efficiently.<sup>11,12</sup> For effective implementation of such devices, we used the work-function-engineered graphene films with an interfacial dipole layer to increase the built-in potential and to improve charge extraction, thereby enhancing the overall device performance.<sup>11,13-17</sup>

Figure 1(a) shows the structure of poly[(9,9-bis((6'-(N,N,N-trimethylammonium) hexyl)-2,7-fluorene)-alt - (9,9-bis(2-(2-methoxyethoxy) ethoxy) ethyl) - 9-fluorene)) dibromide (denoted as WPF-6-oxy-F), which has been reported in detail elsewhere.<sup>18</sup>

This synthesized polymer was used as an interfacial layer to efficiently control the work function of the graphene

film because of its ionic or polar groups that effectively form interface dipoles.<sup>18</sup> Multilayer graphene (MLG) film was grown through chemical vapor deposition (CVD) on nickel films, which has been reported in detail elsewhere.<sup>5</sup> Figures 1(b) and 1(c) show optical and transmission electron microscope (TEM) images, respectively, of the CVD-synthesized MLG film. A high-resolution TEM image of an MLG region containing a ripple [upper inset of Fig. 1(c)] shows the number of graphene layers in the film as well as the interlayer distance. The interlayer spacing was measured as  $3.45 \pm 0.09$  Å. Fig. 1(d) shows the Raman spectra of the CVD-synthesized graphene films grown on Ni and transferred onto Si/SiO<sub>2</sub> substrates. The graphene films exhibited small D-band peaks near  $1350$  cm<sup>-1</sup>, which indicated the high quality of the graphene structures.

The work-function-engineered MLG film was tested using an inverted-structure OSC, as shown in Fig. 2(a). The

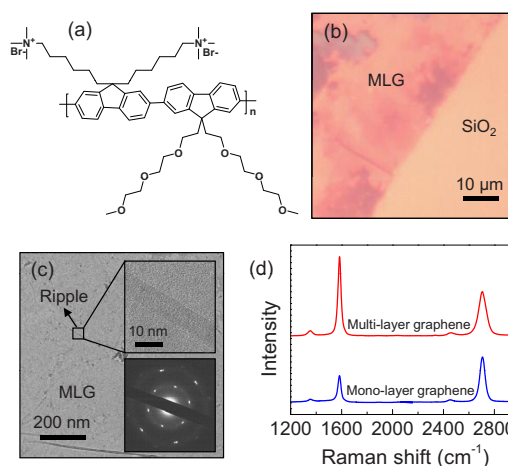


FIG. 1. (Color online) (a) Molecular structure of WPF-6-oxy-F. (b) Optical image of an MLG film. (c) TEM image of an MLG film. The insets show a high-resolution TEM image of the rippled region (upper) and the electron diffraction pattern (lower) of an MLG film. (d) Raman spectra of the MLG films grown on Ni substrate by CVD. The excitation wavelength is 514 nm.

<sup>a)</sup>Electronic mail: yhkahng@gist.ac.kr.

<sup>b)</sup>Electronic mail: tlee@gist.ac.kr.

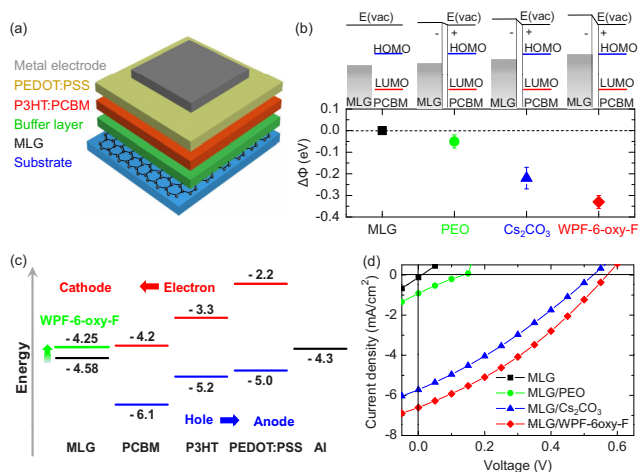


FIG. 2. (Color online) (a) Schematics of an inverted-structure OSC with the work-function-engineered MLG electrode. (b) Changes to the effective work functions ( $\Delta\Phi$ ) of MLG films with interfacial dipole layers. (c) Energy level diagram of the inverted structure OSC with MLG cathode. (d) J-V characteristics of the inverted structure OSCs under illumination with and without the various interfacial layers.

synthesized MLG film was transferred to the glass substrate, and one of the following three types of interfacial dipole layers was spin-coated onto the MLG film: 0.1 wt % solution of poly(ethylene oxide) (PEO) in methanol, 0.2 wt % solution of  $\text{Cs}_2\text{CO}_3$  in 2-ethoxyethanol, or 0.2 wt % solution of WPF-6-oxy-F in methanol. Then, a solution of 30 mg of poly(3-hexylthiophene) (P3HT, Rieke Metal) and 15 mg of 1-(3-methoxycarbonyl)-propyl-1-phenyl-(6,6) $\text{C}_{61}$  (PCBM, Nano-C) in 2 ml of chlorobenzene was spin-coated onto the interfacial layer (thickness  $\sim 90$  nm) and subsequently annealed at  $110^\circ\text{C}$  for 10 min under  $\text{N}_2$ . Poly(3,4-ethylenedioxythiophene):poly(styrenesulfonate) (PEDOT:PSS, Baytron P VPAI 4083) diluted in isopropanol and preheated at  $90^\circ\text{C}$  was spin-coated onto the P3HT:PCBM layer followed by annealing at  $120^\circ\text{C}$  for 10 min under  $\text{N}_2$ , which produced a  $\sim 30$  nm thick layer. Fabrication of the devices was completed by thermal evaporation of an Al anode (100 nm) through a shadow mask at a pressure of  $10^{-6}$  Torr. The photoactive area was defined by the shadow mask ( $4.66\text{ mm}^2$ ). For comparison, devices without any interfacial layers were also fabricated using identical experimental procedures. Finally, photocurrent-voltage (J-V) measurements were performed using a Keithley 4200 instrument under  $100\text{ mA/cm}^2$  illumination from a 1-KW Oriel solar simulator with an AM 1.5 G filter in an  $\text{N}_2$ -filled glove box. A calibrated silicon reference solar cell with a KG5 filter certified by the National Renewable Energy Laboratory was used to confirm the measurement conditions. All of the device performance data presented in this paper represents the average of at least 20 devices.

It is well known that the work functions of the cathode and the lowest unoccupied molecular orbital (LUMO) of the PCBM must be well-matched to form an Ohmic contact and to increase the built-in potential.<sup>13–17</sup> Graphene electrodes coated with a high-work-function layer such as PEDOT:PSS, which forms an Ohmic contact with p-type polymer donor materials, are used for hole extraction (i.e., as anodes) in conventional-structure OSCs.<sup>11</sup> In contrast, we tuned the work function of our graphene electrodes for their use as cathodes in inverted-structure OSCs. To collect electrons at

TABLE I. Changes in the effective work functions of MLG films and ITO films with interfacial dipole layers, and the performance parameters of the OSCs with all types of electrodes.

	$\Delta\Phi$ (eV)	$\eta_p$ (%)	$J_{sc}$ ( $\text{mA/cm}^2$ )	$V_{oc}$ (V)	FF
MLG	...	0	0.12	0.01	0
MLG/PEO	$0.05 \pm 0.03$	0.03	0.92	0.14	0.21
MLG/ $\text{Cs}_2\text{CO}_3$	$0.22 \pm 0.05$	0.89	5.72	0.53	0.30
MLG/WPF-6-oxy-F	$0.33 \pm 0.03$	1.23	6.61	0.57	0.33
ITO	...	0.48	5.27	0.32	0.27
ITO/WPF-6-oxy-F	$0.43 \pm 0.04$	2.23	8.37	0.60	0.44

the cathode effectively, the graphene work function was lowered using an interfacial layer.

To find an appropriate interfacial layer material, we used a Kelvin probe measurement system (KP 6500 Digital Kelvin probe, McAllister Technical Services Co.) to compare the shifts in the work functions of the MLG films after the films made contact with several interfacial layers.<sup>18</sup> Figure 2(b) shows a comparison of the changes in the effective work functions induced by different interfacial layers. The work function of the untreated MLG film was  $4.58 \pm 0.08$  eV, which is close to the work function of highly ordered pyrolytic graphite (HOPG, 4.5 eV).<sup>7</sup> The work function of the MLG film was reduced by the following amounts when the corresponding interfacial dipole layers were used:  $0.05 \pm 0.03$  eV with PEO,  $0.22 \pm 0.05$  eV with  $\text{Cs}_2\text{CO}_3$ , and  $0.33 \pm 0.03$  eV with WPF-6-oxy-F. As illustrated in Fig. 2(b), these interfacial layers formed interfacial dipoles that pointed away from the MLG surface, thereby decreasing the MLG work function. By using different materials, the work function of MLG could be appropriately tuned. For our cathode application, WPF-6-oxy-F was found as the best material because it reduces the effective work function of MLG to a value that is close to the LUMO of PCBM.

Figure 2(c) shows the energy levels of the individual layers and illustrates the operation mechanism of our photovoltaic cell. The work function of pristine MLG (4.58 eV) was reduced to 4.25 eV using a WPF-6-oxy-F interfacial dipole layer. The work function tuning improved the matching between the work functions of MLG and the LUMO of PCBM (4.2 eV), and it increased the built-in potential and charge collection. Figure 2(d) shows the current density-voltage (J-V) data from OSCs fabricated with pristine MLG and work-function-engineered MLG electrodes. In the inverted OSCs with pristine MLG (black symbol), no photovoltaic effect was observed. In this case, the energy level difference between the anode and the cathode, which provides the driving force for the transfer of holes and electrons toward the electrodes, was in reverse alignment.<sup>15</sup> Our results indicate that the work function of the MLG cathode requires changing to produce the necessary charge transfer and collection.<sup>16,17</sup> As the work function of the MLG electrode was reduced further, the solar efficiency improved simultaneously, which demonstrates the importance of engineering the work function of the MLG cathode. The characteristic parameters of all types of OSCs are summarized in Table I. The best performance parameters were obtained with WPF-6-oxy-F as the interfacial layer: short-circuit current density ( $J_{sc}$ ) of  $6.61\text{ mA/cm}^2$ , open circuit voltage ( $V_{oc}$ ) of 0.57 V, and fill factor (FF) of 0.33. These

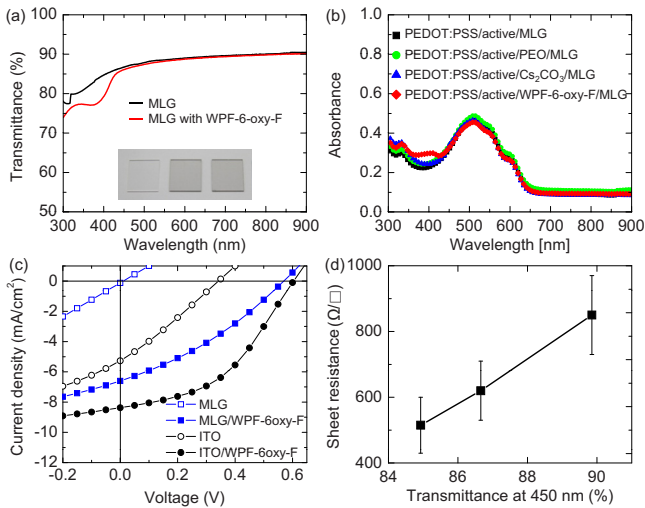


FIG. 3. (Color online) (a) Transmittance spectra of MLG films before and after coating with WPF-6-oxy-F. The inset shows photographs of glass (left), MLG film on glass (middle), and WPF-6-oxy-F-coated MLG film on glass (right). (b) Absorbance spectra of MLG based-OSCs with and without the interfacial layers. (c) J-V characteristics of the inverted OSCs with pristine MLG (open squares), WPF-6-oxy-F functionalized MLG (filled squares), ITO (open circles), and WPF-6-oxy-F functionalized ITO (filled circles). (d) Transmittance vs sheet resistance of MLG films.

values yielded a  $PCE = J_{SC} V_{OC} FF / P_{inc}$  (where  $P_{inc}$  is the power intensity of the incident light) of 1.23%.

Figure 3(a) shows the transmittance spectra of MLG films measured before and after the formation of the WPF-6-oxy-F layer in the visible wavelength range. The inset shows the photograph of glass substrate (left), MLG film on glass (middle), and MLG film coated with WPF-6-oxy-F on glass (right). We found that noncovalent functionalization by WPF-6-oxy-F had a negligible effect on the optical absorption properties of the MLG film in the visible wavelengths, which is expected because the energy gap of WPF-6-oxy-F lies in the UV wavelength range.<sup>8</sup> The absorbance spectra of the MLG based-OSCs with and without the interfacial layers are shown in Fig. 3(b). All of the devices exhibited very similar absorbance spectra. This result indicates that the interfacial layers in the MLG based-OSCs did not significantly increase optical loss, whereas they enhanced the PCE.

Finally, the photovoltaic J-V characteristics of a control device made with a WPF-6-oxy-F functionalized ITO cathode are shown in Fig. 3(c) in comparison with MLG based-devices. The ITO cathode device parameters were  $J_{SC} = 8.37$  mA/cm<sup>2</sup>,  $V_{OC} = 0.60$  V,  $FF = 0.44\%$ , and  $PCE = 2.23\%$ . The PCE of the solar cells with WPF-6-oxy-F functionalized MLG cathodes was 55% of the PCE of cells with WPF-6-oxy-F functionalized ITO electrodes, which may partly be due to the lower sheet resistance of ITO film compared to MLG film. The performance of the OSCs with MLG electrodes is expected to depend strongly on the quality and properties of the MLG film used. Our CVD-synthesized MLG films exhibited high sheet resistance in the range of 850 to 520  $\Omega$ /sq while the transmittance changed from 90% to 85% at a wavelength of 450 nm [Fig. 3(d)]. However, the conductivity of the graphene films can be improved further by several efficient methods for synthesis, transfer, and doping of them.<sup>6,19,20</sup> For example, Bae *et al.* recently developed a highly conductive graphene film with a sheet resistance of  $\sim 30$   $\Omega$ /sq at  $\sim 90\%$  transmittance through layer-by-layer

stacking and chemical doping methods.<sup>20</sup> Furthermore, one of the crucial points needed for practical device applications of OSCs is the stability in ambient condition because conjugated polymers used in our experiments are known to be rather unstable in air, which can be possible by introducing encapsulations, functional layers, and modified device structures.<sup>21</sup> The importance of our findings will be further strengthened with such improvements and stability.

In conclusion, we engineered the work function of MLG films using thin interfacial dipole layers. Graphene films with tuned work functions were used as cathodes in inverted-structure OSCs, which showed improved efficiency. Our demonstration of inverted-structure OSCs with work-function-engineered graphene electrodes will lead to the development of advanced device structures with higher efficiency.

This work was supported by the National Research Laboratory Program, a National Core Research Center grant, the World Class University program from the Korean Ministry of Education, Science, and Technology, the Korea Institute of Science and Technology Institutional Program, and a grant from the Fundamental R&D Program for Core Technology of Materials funded by the Korean Ministry of Knowledge Economy.

<sup>1</sup>K. S. Kim, Y. Zhao, H. Jang, S. Y. Lee, J. M. Kim, K. S. Kim, J.-H. Ahn, P. Kim, J.-Y. Choi, and B. H. Hong, *Nature (London)* **457**, 706 (2009).

<sup>2</sup>G. Eda, G. Fanchini, and M. Chhowalla, *Nat. Nanotechnol.* **3**, 270 (2008).

<sup>3</sup>P. Blake, P. D. Brimicombe, R. R. Nair, T. J. Booth, D. Jiang, F. Schedin, L. A. Ponomarenko, S. V. Morozov, H. F. Gleeson, E. W. Hill, A. K. Geim, and K. S. Novoselov, *Nano Lett.* **8**, 1704 (2008).

<sup>4</sup>G. Jo, M. Choe, C.-Y. Cho, J. H. Kim, W. Park, S. Lee, W.-K. Hong, T.-W. Kim, S.-J. Park, B. H. Hong, Y. H. Kahng, and T. Lee, *Nanotechnology* **21**, 175201 (2010).

<sup>5</sup>L. Gomez De Arco, Y. Zhang, C. W. Schlenker, K. Ryu, M. E. Thompson, and C. Zhou, *ACS Nano* **4**, 2865 (2010).

<sup>6</sup>V. C. Tung, L.-M. Chen, M. J. Allen, J. K. Wassei, K. Nelson, R. B. Kaner, and Y. Yang, *Nano Lett.* **9**, 1949 (2009).

<sup>7</sup>X. Wang, L. Zhi, and K. Mullen, *Nano Lett.* **8**, 323 (2008).

<sup>8</sup>Y. Wang, X. Chen, Y. Zhong, F. Zhu, and K. P. Loh, *Appl. Phys. Lett.* **95**, 063302 (2009).

<sup>9</sup>J. Wu, H. A. Becerril, Z. Bao, Z. Liu, Y. Chen, and P. Peumans, *Appl. Phys. Lett.* **92**, 263302 (2008).

<sup>10</sup>Z. Yin, S. Wu, X. Zhou, X. Huang, Q. Zhang, F. Boey, and H. Zhang, *Small* **6**, 307 (2010).

<sup>11</sup>L.-M. Chen, Z. Hong, G. Li, and Y. Yang, *Adv. Mater. (Weinheim, Ger.)* **21**, 1434 (2009).

<sup>12</sup>J. Y. Kim, K. Lee, N. E. Coates, D. Moses, T.-Q. Nguyen, M. Dante, and A. J. Heeger, *Science* **317**, 222 (2007).

<sup>13</sup>H. Ma, H.-L. Yip, F. Huang, and A. K.-Y. Jen, *Adv. Funct. Mater.* **20**, 1371 (2010).

<sup>14</sup>S.-I. Na, S.-W. Oh, S.-S. Kim, and D.-Y. Kim, *Org. Electron.* **10**, 496 (2009).

<sup>15</sup>H.-L. Yip, S. K. Hau, N. S. Baek, and A. K.-Y. Jen, *Appl. Phys. Lett.* **92**, 193313 (2008).

<sup>16</sup>Y. Zhou, F. Li, S. Barrau, W. Tian, O. Inganäs, and F. Zhang, *Sol. Energy Mater. Sol. Cells* **93**, 497 (2009).

<sup>17</sup>F. Zhang, M. Ceder, and O. Inganäs, *Adv. Mater. (Weinheim, Ger.)* **19**, 1835 (2007).

<sup>18</sup>S.-H. Oh, S.-I. Na, J. Jo, B. Lim, D. Vak, and D.-Y. Kim, *Adv. Funct. Mater.* **20**, 1977 (2010).

<sup>19</sup>X. Li, Y. Zhu, W. Cai, M. Borysiak, B. Han, D. Chen, R. D. Piner, L. Colombo, and R. S. Ruoff, *Nano Lett.* **9**, 4359 (2009).

<sup>20</sup>S. Bae, H. Kim, Y. Lee, X. Xu, J.-S. Park, Y. Zheng, J. Balakrishnan, T. Lei, H. R. Kim, Y. I. Song, Y.-J. Kim, K. S. Kim, B. Özyilmaz, J.-H. Ahn, B. H. Hong, and S. Iijima, *Nat. Nanotechnol.* **5**, 574 (2010).

<sup>21</sup>S. K. Hau, H.-L. Yip, N. S. Baek, J. Zou, K. O'Malley, and A. K.-Y. Jen, *Appl. Phys. Lett.* **92**, 253301 (2008).